MICROSCOPIC AND MACROSCOPIC MODELING OF THERMONUCLEAR BURNING FRONTS

J.C. NIEMEYER
UCO/Lick Observatory, University of California, Santa Cruz, CA 95064, USA

W. HILLEBRANDT
Dep. of Astronomy and Astrophysics, Enrico Fermi Institute, The University of Chicago, Chicago, IL 60637, USA

AND

Max Planck Institut für Astrophysik, Karl Schwarzschild Str.1, 85740 Garching, Germany

1. Introduction

Observational constraints as, for instance, the amount of intermediate mass elements needed to fit SN Ia spectra, in combination with numerical nucleosynthesis calculations imply that if these events are to be explained by thermonuclear explosions of Chandrasekhar mass C+O-white dwarfs, the explosions begin in the subsonic deflagration mode as opposed to supersonic detonations (Woosley 1990). In deflagrations, thin sheets of burning material ("flames") propagate by means of electronic thermal conduction (Timmes & Woosley 1992). On scales larger than a few centimeters the flame is subject to various instabilities that deform its surface, making the macroscopic properties of the wrinkled burning front (the so-called "turbulent flame brush") more complex than, or even independent of, its laminar propagation characteristics (Woosley 1990, Livne 1993, Khokhlov 1993,1994,1995, Niemeyer & Hillebrandt 1995a,b). According to our current knowledge, the turbulent deflagration phase can in principle terminate in three different ways: First, the released energy may be sufficient to unbind the star and produce an explosion which could be compared with SN Ia events. Alternatively, it was suggested that the flame brush makes a transition to a "delayed detonation" after the density has decreased to some 10^7 g cm^{-3} (Khokhlov 1991a,b, Woosley 1994). And, finally, if too little carbon is burned to unbind the star before the flame reaches densities below 10^7 g cm^{-3}, the burning front may re-ignite as either a deflagration or detonation during the re-compression phase and give rise to a successful explosion after one or many pulses (Ivanova *et al* 1977, Arnett & Livne 1994 a,b, Woosley, this volume). In all of these cases, the initial deflagration phase determines the starting conditions for each of the following regimes. It is therefore essential to understand the evolution of the flame brush from the time of its birth at $\rho \approx 2 - 3 \times 10^9$ g cm^{-3} until the late phase at $\rho \approx 10^7$ g cm^{-3}. Particularly interesting in the context of SN Ia models are the thickness of the turbulent flame brush $d_{\rm tur}$, and its overall mass consumption rate which is sometimes expressed in terms of the turbulent flame speed $u_{\rm tur} \propto \dot{X}_{\rm f}\, d_{\rm tur}$, where $\dot{X}_{\rm f}$ denotes the fuel consumption rate. In this work, we will outline some approaches that employ multidimensional hydrodynamic simulations to study turbulent flames in white dwarfs.

The problem of subsonic flame propagation in white dwarfs is made both extremely complicated and highly interesting by the vast range of dynamically relevant scales. Starting at the flame diameter of less than one millimeter and ending at the radius of the white dwarf it covers more than eleven orders of magnitude. This fact prohibits direct numerical simulations of the full problem in the foreseeable future even on the most powerful computers. Numerical hydrodynamicists can thus choose one of two possible simplifications. In the first one, which we will call "small scale calculations" (SSCs) in the following, one attempts to study flame dynamics through a small window in scale space in order to isolate specific physical effects from the environment of the white dwarf. This is usually achieved by imposing constant fuel density and gravity in a box with simple (periodic or reflecting) boundary conditions and assuming a laminar thin flame on all unresolved scales. On the other hand, "large scale calculations" (LSCs) try to simulate the explosion itself on scales of the white dwarf radius. Here, all the information gained by theory and SSCs about flame dynamics on scales below the grid resolution $\Delta_{\rm lsc} \approx 10$ km is used to model the propagation of the turbulent flame brush in a self-gravitating, expanding medium.

Examples of SSCs include the extensive investigation of the Rayleigh-Taylor (RT)-burning regime in two and three dimensions by Khokhlov (1993,1994,1995) and simulations of the Landau-Darrieus-instability by Niemeyer & Hillebrandt (1995a). The former work confirmed numerically that the overall mass consumption rate of a turbulent flame brush is purely determined by hydrodynamical effects if the speed of turbulent or buoyant mixing greatly exceeds the laminar flame speed $u_{\rm lam}$. Obviously, this fact has important implications for numerical flame brush models in LSCs (see section 2). The latter study demonstrated that thermonuclear flames are unstable on scales immediately above the flame thickness owing to the refraction of stream lines at the density jump across the flame. This result has been known for chemical flames since the linear stability analysis of Landau (1944). A more detailed analysis of the nonlinear evolution of the LD-instability and its consequences for SN Ia models was carried out by Blinnikov & Sasorov (1995, see also Blinnikov, this volume).

Multidimensional hydrodynamical LSCs of Chandrasekhar mass explosions were performed by Müller & Arnett (1986), Livne (1993), Arnett & Livne (1994a,b), Khokhlov (1995), and Niemeyer & Hillebrandt (1995b). While all simulations differed to some extent in their prescription for the turbulent mass consumption rate, they all represented the turbulent flame brush in a manner similar to a laminar flame surface, i.e. with a thin, highly peaked energy generation rate profile. We will argue in section (2) that a more realistic treatment is needed in order to account for the fluctuating thickness of the turbulent burning region.

This contribution is structured as follows: First, we briefly summarize some properties of flame propagation in white dwarfs that are relevant for multidimensional simulations. Following this, a series of numerical experiments are presented as an example for recent SSCs. They involve a slightly perturbed flame surface subject to horizontal shear induced by the gravitational acceleration of the burned material with respect to the fuel. One goal of this experiment was to study the effect of the Kelvin-Helmholtz (KH)-instability on the formation of cellular structures during the nonlinear evolution of the LD-instability. Section (4) is devoted to describe a new approach to model the macroscopic features of a nuclear flame brush in LSCs by means of heat transport with a turbulent subgrid diffusion coefficient. Finally, some results of this method and their relation to earlier simulations will be discussed.

2. Properties of the turbulent flame brush

At densities above 10^7 g cm^{-3}, the speed of laminar deflagration fronts ("flames") $u_{\rm lam}$ in degenerate C+O-matter is known to be of the order of some percent of the sound speed, while the thickness of their thermal diffusion region $l_{\rm th}$ is smaller than $\approx$ 1 cm (Timmes & Woosley 1992). Moreover, these flames are unstable on all scales above $\approx 100\, l_{\rm th}$, where the intrinsic Landau-Darrieus (LD)-instability dominates on the smaller length scales, while the buoyancy-driven Rayleigh-Taylor (RT)-instability becomes the most important dynamical effect on large scales. Immediately after the formation of buoyant RT-bubbles the Kelvin-Helmoltz (KH)-instability of tangetial velocity gradients along the bubble walls gives rise to the onset of unstabilized, isotropic turbulence that dominates flame dynamics on all scales down to the Gibson scale $l_{\rm gibs}$, where $u_{\rm lam}$ is equal to the characteristic turbulent velocity

$$v(l_{\rm gibs}) = u_{\rm lam} \tag{1}$$

(Niemeyer & Hillebrandt 1995b). In the early and main phase of the explosion one can estimate the Gibson scale to be of the order of 10^4 cm (Niemeyer & Hillebrandt 1995b). This burning regime, characterized by the large separation of $l_{\rm th}$ and $l_{\rm gibs}$, is called the "corrugated flamelet regime" (e.g., Clavin 1994). As the flame crossing time $\tau_{\rm fc} = l/u_{\rm lam}$ is shorter than the eddy turnover time $\tau_{\rm eddy}(l) = l/v(l)$ on all scales $l < l_{\rm gibs}$, the Gibson scale defines a lower bound for the curvature radius of flame wrinkles caused by turbulent stress. Thus, if $l_{\rm th} \ll l_{\rm gibs}$, small segments of the flame surface are unaffected by large scale turbulence and behave as unperturbed laminar flames ("flamelets"). If, in addition, there exists a wide range of scales where the turbulent fluctuations exceed the laminar burning speed, i.e., the integral scale of turbulence $L \gg l_{\rm gibs}$, one can argue that inside this range both transport and burning times are determined by the eddy turnover time $\tau_{\rm eddy}(l)$ (Kerstein 1988, Clavin 1990). Hence, when measured at the largest turbulent scale L, the speed and thickness of the burning front are given by:

$$u_{\rm tur}(L) \approx v(L) \quad , \quad d_{\rm tur}(L) \approx L \; . \tag{2}$$

Since in the case of turbulence produced by floating RT-bubbles L is of the order of $10^6 - 10^7$ cm, the flame front in SN Ia models satisfies the conditions listed above during most of the explosion. In particular, all properties of the turbulent flame front become independent of microphysical aspects, such as the temperature dependence of nuclear burning and electronic conduction. It is the behavior of this so-called "turbulent flame brush" that we want to study. One of the main goals of this work is to find a way to model the turbulent flame brush in large scale simulations without any *a proiri* assumption about its thickness and energy generation rate profile.

One important aspect of thermonuclear flamelets is their persistence: Once ignited, even the smallest flame fragments survive when separated from larger sheets as long as $l_{\rm th} \ll l_{\rm gibs}$. Therefore, when burning material is transported into unburned matter ahead of the flame brush, fresh fuel is ignited immediately. Propagation of the flame brush boundary is thus limited by contamination of the unburned region with flamelets. The ignition of fresh fuel ahead of a *laminar* flame, on the other hand, is limited by the high activation temperature of the nuclear reactions. It is responsible for the strongly localized reaction region $l_{\rm reac,lam}$ of laminar flames which is much smaller than the thermal diffusion zone ($l_{\rm reac,lam} \ll l_{\rm th,lam}$). Owing to the transport limited ignition of *turbulent* nuclear burning fronts we may expect a much broader reaction rate profile in this case: $l_{\rm reac,tur} \approx l_{\rm th,tur}$ (Clavin 1990).

In order to evaluate the largest scale where flame properties are determined by isotropic turbulence we must consider the source of the turbulent cascade, the RT-instability. To find upper bounds for L and $v(L)$ we note that turbulent velocities are roughly limited by the fastest shear flows which, in turn, are limited by the rise velocity of the largest burning bubbles $v_{\rm rt}$. For a spherical bubble it is given by

$$v_{\rm rt} = \mathcal{B}\,\sqrt{g_{\rm eff} l}\ , \tag{3}$$

(Layzer 1955) where $\mathcal{B} \approx 0.511$ is a constant, $g_{\rm eff} = At\,g$ is the effective gravitational acceleration, the Atwood number $At = (\rho_{\rm u} - \rho_{\rm b})/(\rho_{\rm u} + \rho_{\rm b})$ is a measure for the density contrast of burned and unburned fluids, and l is the radius of the bubble. On the largest scales, however, the development of turbulence is inhibited by expansion of the star during the explosion. As pointed out by Khokhlov (1995), turbulent eddies become "frozen" if the medium expands on a shorter timescale than the eddy rotates. We can thus estimate the largest length scale where turbulent mixing occurs to be the length $l_{\rm tur,max}$ whose eddy turnover time is equal to the hydrodynamical timescale of the white dwarf, $\tau_{\rm dyn} \approx 0.1$ s. Together with equation (3) we find:

$$l_{\rm tur,max} = \tau_{\rm dyn}^2\,\mathcal{B}^2\,g_{\rm eff} \approx 10^6\ {\rm cm}\ , \tag{4}$$

where we have used $g_{\rm eff} \approx 5 \times 10^8\ {\rm cm/s^2}$ as a typical value for the effective acceleration. All structures larger than $l_{\rm tur,max}$ will evolve on a comparable (or slower) timescale with the overall expansion and consequently have to be simulated directly by means of multidimensional numerical hydrodynamics, implying a grid resolution $\Delta \lesssim l_{\rm tur,max}$. On the other hand, on scales smaller than $l_{\rm tur,max}$ we can legitimately employ a phenomenological model based on the statistical behavior of fully developed turbulence for the turbulent fluctuations on subgrid (SG) scales, as will be described in section (4).

3. Burning fronts in the presence of shear

A set of two-dimensional hydrodynamical SSCs was carried out using the PPM-based program PROMETHEUS (Fryxell *et al* 1989). All calculations took place on a Cartesian grid with 100×100 zones, periodic boundary conditions at both y-ends, and reflecting and outflow conditions at the left and right x-boundaries, respectively. We employed a simple algorithm to model a flame that propagates toward the unburned material with a constant flame velocity and thickness. The code detects the gradient of C+O-material and allows nuclear burning in the three zones closest to a lower fuel cut-off ($X_{\rm C+O} \approx 10^{-3}$), while the burning rate is determined by the pre-defined laminar flame speed $u(\Delta)$ (see Niemeyer & Hillebrandt 1995b for details). One-dimensional tests were applied to calibrate the numerical flame speed.

In all simulations a flame front propagates across the grid in the positive x-direction. It is ignited by instantly turning the composition of the innermost ten zones into nickel and adding the liberated binding energy of $\epsilon_{\rm nuc} \approx 7 \times 10^{17}$ erg/g to their internal energy. The initial flame surface is perturbed sinusodially with an amplitude of three zones and varying wavelengths in order to compensate for the decreasing grid-crossing times of increasingly rapid shear flows. During the simulation, all burned material is accelerated upward relative to the unburned matter that remains vertically at rest in the numerical frame of reference. In addition, a simple drag force is included in order to provide a constant asymptotic rise velocity of the hot fluid. Thus, buoyant acceleration is parameterized by:

$$\frac{dv_y}{dt} = g_{\rm eff} - C_{\rm d}\, v_y \ , \tag{5}$$

where the coefficient $C_{\rm d}$ is a free parameter determined by the final shear velocity $v_{\rm kh}$:

$$C_{\rm d} = v_{\rm kh}^{-1}\, g_{\rm eff} \ . \tag{6}$$

Since the origin of acceleration is irrelevant for the actual simulation we can also interpret this model in terms of interacting turbulent eddies with a relative velocity $v_{\rm kh}$. In this case, the minimum value of $v_{\rm kh}/u_{\rm lam} \equiv Z$ for which the flame is fully unstable (i.e., no nonlinear stabilization is active) is directly linked to the Gibson scale by equation (1).

The goal of our simulations was to investigate the development of small initial perturbations as a function of varying Z. In fact, according to the discussion above it is clear that Z is the dominant parameter that governs the behavior of flames subject to shear. The only additional physical quantity that enters the model is the effective gravitational acceleration $g_{\rm eff}$ that is essentially determined by the local density contrast and the geometry of the observed buoyant structure. In our specific case it only affects the thickness of the acceleration layer where v_y changes from zero to $v_{\rm kh}$, so that increasing gravity can be expected to destabilize the flame by steepening the tangential velocity gradient. In the white dwarf, this coincides with moving radially outward where g increases and degeneracy becomes less pronounced, thereby increasing $\Delta\rho/\rho$. However, we restrict our investigation to a constant value of $g_{\rm eff} \approx 5 \times 10^8$ cm/s^2. Furthermore, the physical conditions are modeled as encountered by the flame at a density of $\rho_{\rm u} = 5 \times 10^8$ g cm^{-3} in a $X_{\rm C}/X_{\rm O} = 0.3/0.7$-composition, where the laminar flame speed is $u_{\rm lam} \approx 1.9 \times 10^6$ cm/s. These quantities, as well as the size of the grid ($L_{\rm grid} = 4 \times 10^7$ cm in both directions), remain unchanged throughout the simulations in order to isolate the effects of Z-variations.

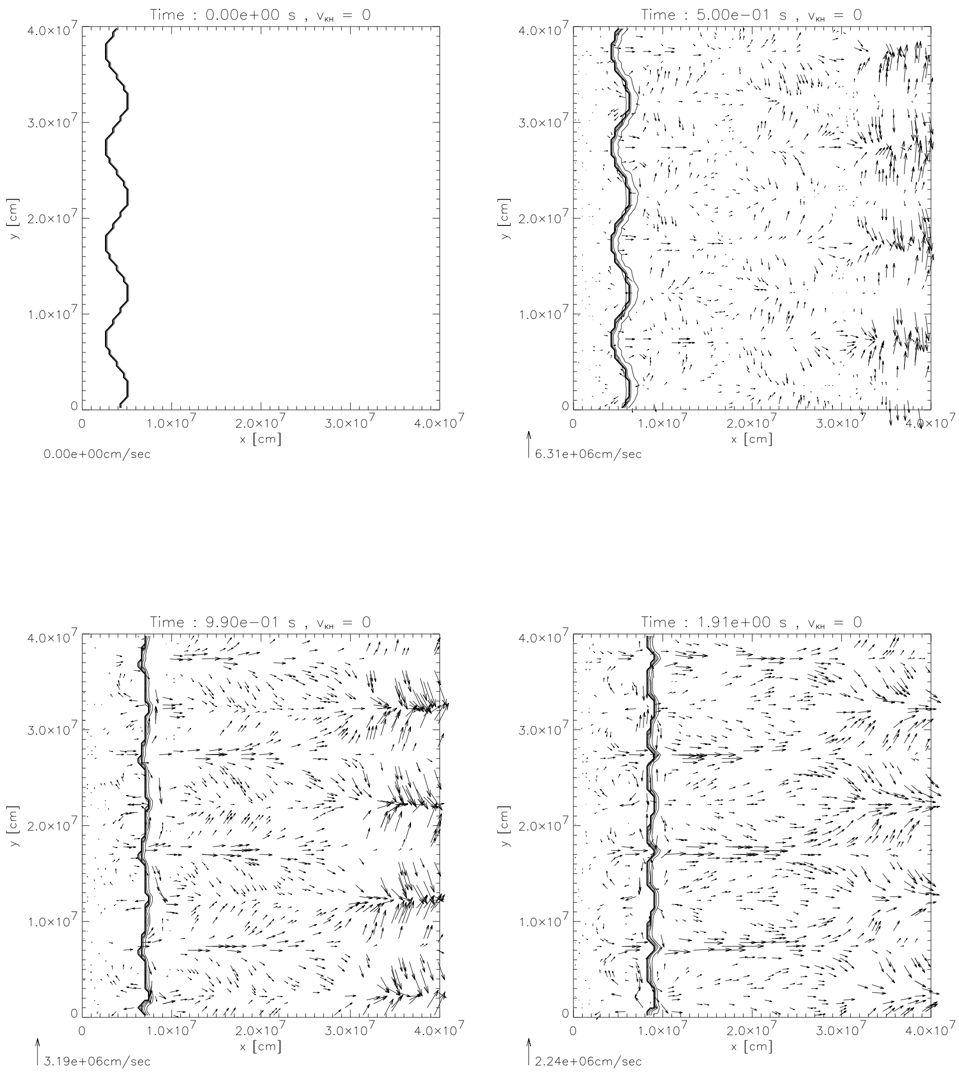

Figure 1. Evolution of a perturbed laminar flame front without shear. The contour lines depict the C+O-mass fraction at logarithmic intervals.

In the first case that was studied we set $Z = 0$, corresponding to a common laminar flame surface propagating under weightless conditions. Figure (1) shows the shape of the flame front at four different times. Only one second after flame ignition the original perturbations have been damped to small wrinkles on an almost flat flame surface. These distortions, however, remain undamped and even grow slightly within the following second. They form a fluctuating small scale pattern with an approximately stationary

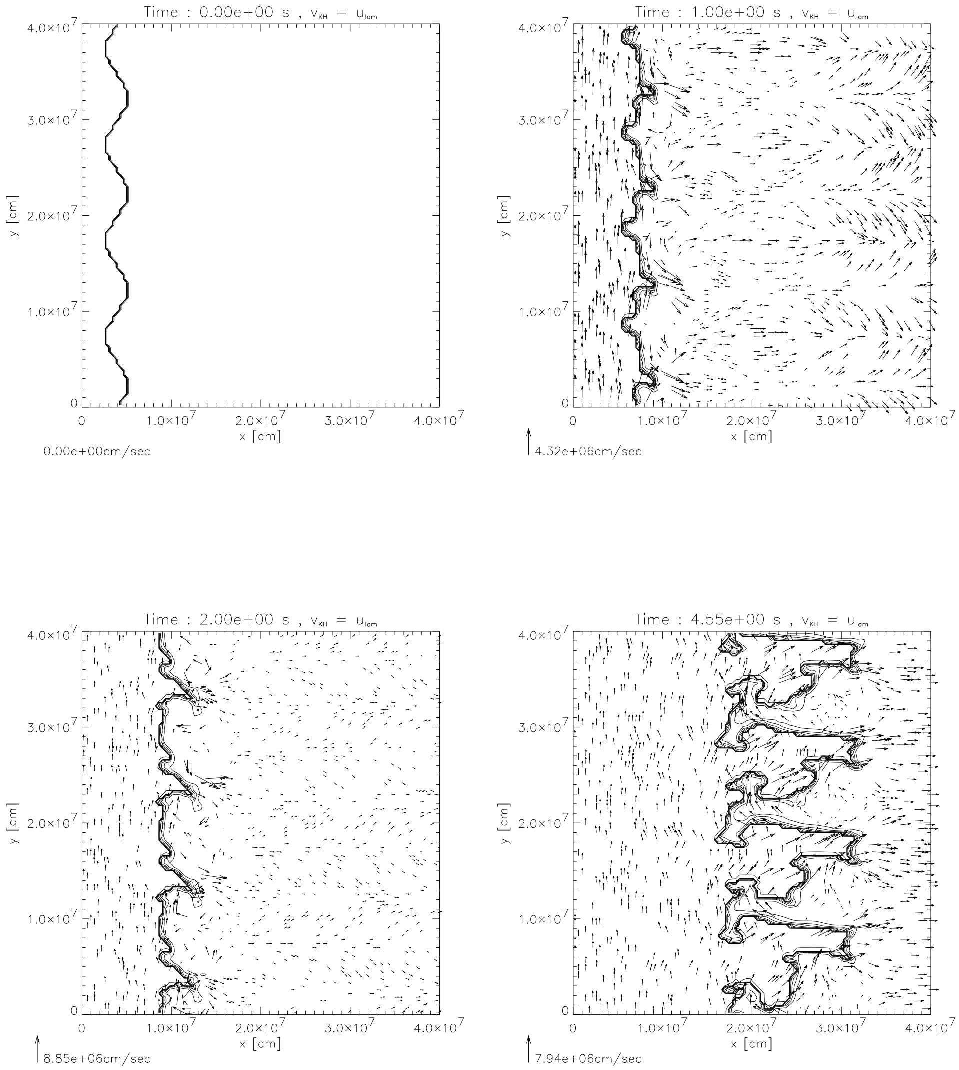

Figure 2. Flame evolution for a shear velocity equal to the laminar burning speed ($Z = 1$).

amplitude, the so-called "cellular regime". It arises from the competition of the (linear) LD-instability and the (nonlinear) damping effect of intersecting flame segments. Notice, however, that the artificial numerical flame thickness strongly affects pattern formation on scales of l_{th}. Nevertheless, it can safely be stated that the flame surface shows only small excursions from its laminar state and therefore moves at a speed only marginally higher than u_{lam}. This is a direct consequence of the nonlinear self-stabilization effect of LD-unstable flames (Zeldovich *et al* 1985, Khokhlov 1995).

The second calculation, where $Z = 1$ (fig. 2), demonstrates one of the key results of this section: The nonlinear stabilization effect breaks down in the presence of shear. The reason is obvious: instead of forming cusps that are able to catch up with the crests of the perturbation wave by moving in a parallel direction, the perturbations here are constantly deformed and bent away from the direction of flame propagation by the shear flow. It is difficult to assess whether the observed front evolution is directly related to the KH-instability or rather a consequence of the LD-instability when self-stabilization is removed. The answer probably includes both aspects, varying continuously from LD to KH dominated dynamics with increasing Z. The case of $Z = 1$ indeed appears to mark a transition point, since the flame does not become turbulent even after a period of $t = 4$ s, in spite of still growing perturbations. This point has been confirmed by additional simulations of cases with $Z > 1$ which show the development of turbulence, as described in (Niemeyer 1995).

Finally, these results have some implications for the lower cut-off scale of the turbulent burning regime. As briefly pointed out above, a situation similar to the one modeled in our simulations occurs if a flame segment encounters an unburned fluid element that has a relative tangential velocity of v_{kh}. The observed amplification of flame perturbations for $Z = 1$ implies that flame dynamics begin to be strongly affected by turbulent motions at scales equal to or above the Gibson scale (1). Evidently, our numerical results confirm the validity of the Gibson scale as the lower limit for turbulent burning.

4. Macroscopic modeling of thermonuclear burning fronts

Numerical LSCs of flame front dynamics in SN Ia explosions also rely on multidimensional (2D and, recently, 3D) explicit hydrodynamical codes. In the commonly applied "finite difference schemes" the hydrodynamical equations are discretized in space and integrated by advancing their variables over short time steps. Discretization usually involves a spatial grid whose cell size will be denoted by the linear length Δ hereafter. As a consequence of spatial discretization, information about scales below Δ cannot be obtained directly from the large scale simulation. Every finite difference scheme applies a low-pass filter of some sort in order to consistently model the evolution of the macroscopic hydrodynamical variables $\bar{\rho}_\Delta$, $\bar{\mathbf{v}}_\Delta$, $\bar{X}_{i\Delta}$, and $\bar{e}_\Delta$. In case of the method employed in this work, the "Piecewise Parabolic Method" (PPM), this is done by imposing a monotonicity constraint on the interpolation routine that computes cell-boundary values from those at the centers (Colella & Woodward 1984). The resulting hydrodynamical variables correspond to the physical ones, smoothed at the grid scale Δ. An assumption that is thus implicitly accepted by every finite difference model is the validity of the equation of state (EOS) for the smoothed variables:

$$\bar{T}_\Delta(\rho, e, X_{i_\Delta}) = T(\bar{\rho}_\Delta, \bar{e}_\Delta, \bar{X}_{i_\Delta}) \ , \tag{7}$$

where the *rhs* is given numerically by the EOS of the model and the *lhs* is the value required by self-consistency. Notice that (7) is only a good approximation in the absence of strong gradients within one cell and therefore, strictly speaking, breaks down for zones that contain part of the flame surface, independent of the specific flame propagation technique.

The need for a special numerical treatment of the flame becomes immediately evident if one considers the total energy generation rate $\int_{V_\Delta} d^3x\, \rho\dot{S}$ of one zone: clearly, it cannot be calculated from the unmodified nuclear rate equations if the flame is not fully resolved. In other words,

$$\int\limits_{V_\Delta} d^3x\, \rho\dot{S}(\rho, T, X_{i_\Delta}) \neq \bar{\rho}_\Delta\, \Delta^3\, \dot{S}(\bar{\rho}_\Delta, \bar{T}_\Delta, \bar{X}_{i_\Delta}) \ , \tag{8}$$

because the *rhs*, included in the large scale hydrodynamical equations, implies that burning occurs at a constant rate, determined by $\bar{T}_\Delta$, throughout the zone. Since $\bar{T}_\Delta$ quickly rises to the final temperature T_b after the flame enters the zone because of the low specific heat capacity of degenerate matter and assumption (7), the *rhs* of equation (8) corresponds to homogeneous burning at the maximum rate of the laminar flame in a volume $V_\Delta \approx \Delta^3$. On the other hand, the physical volume of nonzero energy generation is the product of the flame surface and the thickness of the reaction zone: $V_\mathrm{r} = A_\mathrm{flame} l_\mathrm{r}$. In the flamelet regime, $V_\mathrm{r} \ll \Delta^3$ and thus the *lhs* of equation (8) is much smaller than the *rhs*. As a consequence, in order to realistically calculate the smoothed energy generation rate $\overline{\left(\rho\dot{S}\right)}_\Delta(\mathbf{x}, t)$ at each grid point, a phenomenological model for the location, thickness, and propagation properties of the turbulent flame brush is required.

As described by (Niemeyer & Hillebrandt 1995b) and (Hillebrandt & Niemeyer, this volume), one possibility to obtain information about turbulent velocity fluctuations on the grid scale is to employ a subgrid (SG) model for the unresolved turbulent kinetic energy $q \propto v(\Delta)^2$. It can be modeled with a transport equation that includes a source term related to the stress tensor of the resolved velocity field and a sink term that parameterizes microscopic viscous dissipation. One may interpret this quantity as a measure for the local strength of turbulent fluctuations on the grid scale including a "memory" for the fluid element history.

The SG-model provides the turbulent viscosity coefficient $\nu_\mathrm{tur} \propto q^{1/2}\Delta$ which dominates over all microscopic transport processes if, as in our case,

$v(\Delta) \gg u_{\rm lam}$. Hence turbulent transport of internal energy $\epsilon_{\rm i}$ can be parameterized by a diffusion ansatz:

$$\begin{aligned} \mathbf{h} &= \rho C_{\epsilon_{\rm i}} \nu_{\rm tur} \nabla \epsilon_{\rm i} \\ &= \rho C_{\epsilon_{\rm i}} \nu_{\rm tur} c_p \nabla \bar{T}_\Delta \end{aligned} \tag{9}$$

if the specific heat c_p is assumed to be locally constant. The constant $C_{\epsilon_{\rm i}}$ is of order unity; it has been calibrated by numerical tests to provide energy diffusion as required for modeling the flame front (Niemeyer 1995). This way, it becomes possible to model the propagation of the turbulent flame brush in a manner identical to laminar flames, with the microscopic heat conduction coefficient replaced by $\rho C_{\epsilon_{\rm i}} \nu_{\rm tur} c_p$. However, as emphasized above the temperature dependent nuclear rate equations are unsuitable to calculate the energy generation rate in the flamelet regime as long as the flame is unresolved. Consequently, we use the temperature of a zone only to determine whether or not the fluid element (or some part of it) has reached the flamelet burning mode, in which case $\dot{S}$ can be derived from the turbulent flame speed (see below). The burning mode in each zone can be evaluated by comparing the thickness of a (laminar or turbulent) flame at the burning temperature $\bar{T}_\Delta$ with the grid resolution Δ and switching from nuclear to flamelet mode roughly at the point where the flame becomes unresolved. Details of this method are described in (Niemeyer 1995).

In the flamelet mode, the effective energy generation rate in each zone can be derived from $v(\Delta) \propto q^{1/2}$ with the help of equation (2). Here, we have to take into consideration that mixing caused by unresolved RT-bubbles may exceed turbulent mixing under certain circumstances. In this case, it dominates the fuel consumption rate according to the discussion of equation (2). In addition, both turbulent and buoyant mixing can be slower than the laminar flame speed immediately after ignition. The effective burning speed is therefore given by

$$u_{\rm tur}(\Delta) = \max(u_{\rm lam}, v(\Delta), v_{\rm rt}) \ , \tag{10}$$

and the energy generation rate on the grid scale can be calculated from

$$\overline{\left(\rho \dot{S}\right)}_\Delta \equiv \frac{1}{\Delta^3} \int\limits_{V_\Delta} d^3x \, \rho \dot{S} \approx \frac{u_{\rm tur}(\Delta) \bar{\rho}_\Delta \epsilon_{\rm nuc}}{\Delta} \ , \tag{11}$$

where V_Δ is the volume of the grid cell and $\epsilon_{\rm nuc} = 7 \times 10^{17}$ erg/g stands for the net nuclear energy released by burning carbon to nuclear statistical equilibrium (NSE). The end of flamelet burning is, of course, determined by fuel depletion.

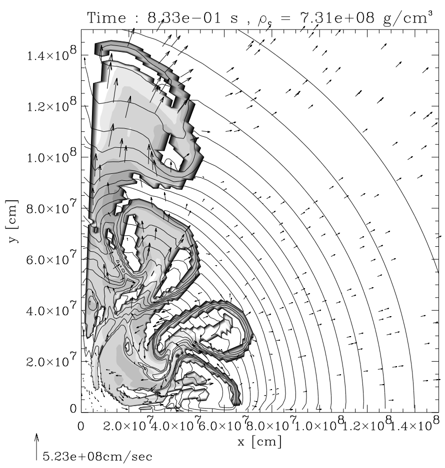

Figure 3. Core region in the central ignition model 0.8 s after ignition. Density contours are separated by $\delta\rho = 3 \times 10^6$ g cm^{-3}, the maximum energy generation rate shown is $\dot{S}_{\max} = 1.3 \times 10^{19}$ erg g^{-1} s^{-1}.

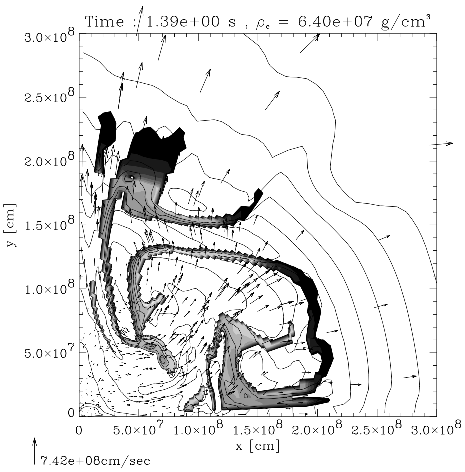

Figure 4. $\delta\rho = 5 \times 10^6$ g cm^{-3}, $\dot{S}_{\max} = 1.1 \times 10^{19}$ erg g^{-1} s^{-1}.

5. Some results of turbulent flame simulations

Employing the turbulent flame brush model we carried out a number of two-dimensional simulations of the deflagration phase of Type Ia supernovae with varying initial conditions. The flame propagation scheme was implemented in the PPM code PROMETHEUS (Fryxell *et al* 1989) in combination with the SG-model for unresolved turbulence (Niemeyer & Hillebrandt 1995b). As a first example, fig. (3) represents the flame brush 0.8 s after ignition for the case of a centrally ignited region with an initial flame surface perturbed by a single sine curve. The development of RT-bubbles is well known (e.g., Khokhlov 1995), but in contrast with earlier simulations of the same process the burning front develops regions where the front thickness differs substantially from its mean value of approximately 5 zones. This interesting property of the flame brush is caused by local variations of the SG-quantities $\nu_{\rm tur}$ and $u_{\rm tur}$ which are responsible for front propagation and fuel digestion. Most of the shear that gives rise to SG-turbulence is created along the boundaries of floating bubbles while the flame brush itself is assumed to behave passively, i.e. the production of q is turned off inside the front. Hence, front propagation at the boundary often exceeds fuel consumption further inside, causing the flame brush to become significantly thicker in some areas. Despite the apparent numerical nature of this effect one can argue that the resulting flame brush structure

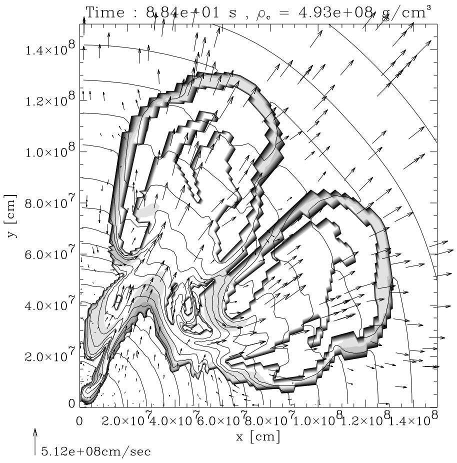

Figure 5. $\delta\rho = 3 \times 10^7$ g cm^{-3}, $\dot{S}_{\rm max} = 10^{19}$ erg g^{-1} s^{-1}.

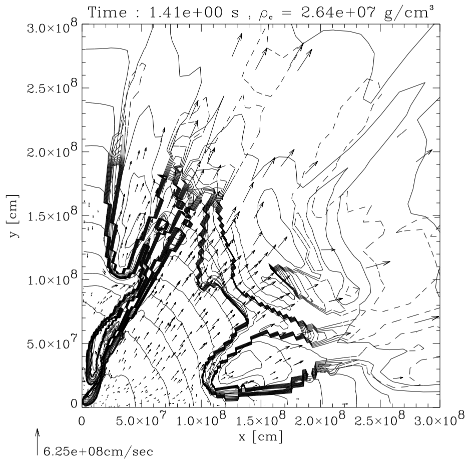

Figure 6. $\delta\rho = 2 \times 10^6$ g cm^{-3}, $\delta\dot{S} = 5 \times 10^{17}$ erg g^{-1} s^{-1} and $\dot{S}_{\rm max} = 6 \times 10^{18}$ erg g^{-1} s^{-1}.

is a qualitatively correct description of reality if the assumption of a purely passive flame front is justified. The latter question is far from being settled at present (Niemeyer & Woosley 1995) and will have to be reconsidered in future studies.

Near the end of the deflagration phase the star has expanded to a density of $\rho \approx 10^7$ g cm^{-3} (fig. 4). Only a small region remains burning in the flamelet mode. During the explosion the turbulent flame speed never exceeded $u_{\rm tur} \approx 2 \times 10^7$ cm/s, which is consistent with the RT-speed at $l \approx \Delta$ that is the main source of SG-turbulence. However, the star has burned approximately 0.6 $M_\odot$ of carbon to nickel, enough to produce a weak supernova (although the large amount of unburned C+O would probably agree poorly with SN Ia spectra).

By using different initial conditions for the flame ignition, specifically by igniting at multiple points off-center (as proposed by Garcia & Woosley 1995), the final nickel mass can be increased to ≈ 0.7 $M_\odot$. This effect is related to the larger initial flame surface and higher material velocities at early times. Since the burning bubbles are now allowed to float freely immediately after ignition without having to overcome the linear RT-growth phase they reach a higher radial distance from the center within the first second of the explosion (figs. 5 and 6). More material is burned at densities below $\approx 10^7$ g cm^{-3} and, consequently, one may expect a higher yield of intermediate mass isotopes from off-center ignitions than from central ignition models. Still, none of our model was able to reproduce a powerful, bright SN Ia that requires burning of up to 1 $M_\odot$ of carbon. Taken at face value, the implications of these results are intriguing: the initial deflagration phase burns too much mass to become a pulsational detonation since the star is definitely unbound. On the other hand, passive turbulent combustion alone appears to be unable to produce sufficiently energetic explosions to account for the whole class of SN Ia's. We therefore need to find a physical explanation that predicts burning of either significantly less or more material during the deflagration phase. While the results of Khokhlov (1995, see also Wheeler, this volume) clearly suggest the former alternative, a higher burning rate may be obtained from additional sources of turbulence such as active turbulent combustion or differential rotation. These topics will have to addressed carefully before any definite statements on the fate of the deflagration phase can be made.

6. Conclusions

Multidimensional hydrodynamical simulations have become an indispensable tool for the investigation of the turbulent deflagration phase of SN Ia models. Small scale calculations of representative length scales allow us to study pieces of the flame surface under microscopes with different resolutions. Here, the challenge is to address general questions in a specific numerical framework without contaminating the answers with artificially imposed initial and boundary conditions. Starting from these results we can try to extrapolate the flame properties over the ten or more orders of magnitude of relevant length scales. Including these models in large scale simulations of the exploding star presents difficulties of a different sort. The theoretical properties the turbulent flame brush which are true – if at all – only in a statistical sense now need to be translated into local realizations of the macroscopic energy generation and front propagation rate. An important aspect of this difficult task is to find a numerical representation of the flame brush that is both grid independent and able to appropriately describe flame propagation in both radial and angular direction.

In this contribution, we have introduced examples for small and large scale calculations in two dimensions. The emergence of flame instabilities by shear flow along the flame surface was demonstrated numerically. The result for the minimum unstable shear velocity suggests that the cellular stabilization mechanism of the LD-instability becomes unimportant at the Gibson scale where the turbulent shear is comparable to the laminar flame speed. On scales of the whole star, simulations with a phenomenologically motivated flame brush model present the picture of a highly anisotropic turbulent burning front with a strongly fluctuating thickness. If the flame is ignited at several points off-center, burning bubbles can be seen floating toward the surface with high speeds from very early on. As a result, the production of both nickel and intermediate mass elements is enhanced with respect to the case of central ignition. Nevertheless, the energetic yield of these models is insufficient to explain the light curves and ejecta velocities of typical Type Ia supernovae. One may interpret this result either as a confirmation for the need for a delayed detonation (or a pulsational one, if the star remains bound), or as one more step toward an explosion mechanism purely driven by turbulent combustion. For the latter case, however, additional physics would have to be invoked in order to increase the efficiency of turbulent flame propagation. In any case, the turbulent deflagration phase of Chandrasekhar mass SN Ia's is a phenomenon that is at best marginally understood, and its exploration will continue for some time to raise challenging questions.

Acknowledgements

It is our pleasure to thank Stan Woosley for numerous discussions about nuclear flames and SN Ia models, Sergej Blinnikov for conversations about microscopic flame dynamics, and Ewald Müller for his assistance with PROMETHEUS. Part of this work was carried out at the University of California in Santa Cruz, whose hospitality we thankfully acknowledge. One of us (JCN) received support from a German Exchange Service fellowship HSP II / AUFE.

References

1. Arnett, W.D., Livne, E.: 1994a, *Astrophys. J.*, **427**, 315
2. Arnett, W.D., Livne, E.: 1994b, *Astrophys. J.*, **427**, 330
3. Blinnikov, S.I., Sasorov, P.V.: 1995, *Preprint*, subm. to *Phys. Rev. E*
4. Clavin, P.: 1990, in *Fluid dynamical aspects of combustion theory*, eds. M. Onofri & A. Tesei, Longman, Harlow, p.43
5. Clavin, P.: 1994, *Annual Rev. Fluid Mech.*, **26**, 321
6. Colella, P., Woodward, P.R.: 1984, *J. Comput. Phys.*, **54**, 174
7. Fryxell, B.A., Müller, E., Arnett, W.D.: 1989, *MPA Preprint Series*, **449**
8. Garcia, D., Woosley, S.E.: 1995, *Astrophys. J.*, **454**, in press
9. Ivanova, L.N., Imshennik, V.S., & Chechetkin, V.M.: 1977, *Astron. Zh.* , **54**, 661; see also *Sov. Astron.*, **21**, 374
10. Kerstein, A.: 1988, *Combust. Sci. Tech.*, **50**, 441
11. Khokhlov, A.M.: 1991a, *Astr. Astrophys.*, **245**, 114
12. Khokhlov, A.M.: 1991b, *Astr. Astrophys.*, **245**, L25
13. Khokhlov, A.M.: 1993, *Astrophys. J. Lett.*, **419**, L77
14. Khokhlov, A.M.: 1994, *Astrophys. J.*, **424**, L115
15. Khokhlov, A.M.: 1995, *Astrophys. J.*, **449**, 695
16. Landau, L.D.: 1944, *Acta Physicochim. URSS*, **19**, 77
17. Layzer, D.: 1955, *Astrophys. J.*, **122**, 1
18. Livne, E.: 1993, *Astrophys. J. Lett.*, **406**, L17
19. Müller, E., Arnett, W.D.: 1986, *Astrophys. J.*, **307**, 619
20. Niemeyer, J.C.: 1995, *Ph.D. Thesis*, *MPA Preprint Series*, **911**
21. Niemeyer, J.C., Hillebrandt, W.: 1995a, *Astrophys. J.*, **452**, 779

22. Niemeyer, J.C., Hillebrandt, W.: 1995b, *Astrophys. J.*, **452**, 769
23. Niemeyer, J.C., Woosley, S.E.: 1995, submitted to *Astrophys. J.*
24. Timmes, F.X., Woosley, S.E.: 1992, *Astrophys. J.*, **396**, 649
25. Woosley, S.E.: 1990, in *Supernovae*, ed. A.G. Petschek, p.182, Springer-Verlag, Berlin
26. Woosley, S.E.: 1994, in *Supernovae*, eds. S.A. Bludmann, R. Mochkovitch, J. Zinn-Justin, Elsevier Science, Amsterdam
27. Zeldovich, Y.B., Barenblatt, G.I., Librovich, V.B., Makhviladze, G.M.: 1985, *The Mathematical Theory of Combustion and Explosions*, Plenum, New York